Cellular/Molecular

Neuroligin 1 Is Dynamically Exchanged at Postsynaptic Sites

Inga U. Schapitz,[1]* Bardo Behrend,[1]* Yvonne Pechmann,[1] Corinna Lappe-Siefke,[1] Silas J. Kneussel,[1] Karen E. Wallace,[3] A. Vanessa Stempel,[5] Fritz Buck,[2] Seth G. N. Grant,[4] Michaela Schweizer,[1] Dietmar Schmitz,[5] Jürgen R. Schwarz,[1] Erika L. F. Holzbaur,[3] and Matthias Kneussel[1]

[1]Center for Molecular Neurobiology (ZMNH), University of Hamburg Medical School, D-20251 Hamburg, Germany, [2]Institute of Clinical Chemistry, University of Hamburg Medical School, D-20246 Hamburg, Germany, [3]Department of Physiology, University of Pennsylvania, School of Medicine, Philadelphia, Pennsylvania 19104, [4]Wellcome Trust Sanger Institute, Hinxton CB10 1SA, United Kingdom, and [5]Neuroscience Research Center of the Charité, Universitätsmedizin Berlin, D-10117 Berlin, Germany

Neuroligins are postsynaptic cell adhesion molecules that associate with presynaptic neurexins. Both factors form a transsynaptic connection, mediate signaling across the synapse, specify synaptic functions, and play a role in synapse formation. Neuroligin dysfunction impairs synaptic transmission, disrupts neuronal networks, and is thought to participate in cognitive diseases.

Here we report that chemical treatment designed to induce long-term potentiation or long-term depression (LTD) induces neuroligin 1/3 turnover, leading to either increased or decreased surface membrane protein levels, respectively. Despite its structural role at a crucial transsynaptic position, GFP-neuroligin 1 leaves synapses in hippocampal neurons over time with chemical LTD-induced neuroligin internalization depending on an intact microtubule cytoskeleton. Accordingly, neuroligin 1 and its binding partner postsynaptic density protein-95 (PSD-95) associate with components of the dynein motor complex and undergo retrograde cotransport with a dynein subunit.

Transgenic depletion of dynein function in mice causes postsynaptic NLG1/3 and PSD-95 enrichment. In parallel, PSD lengths and spine head sizes are significantly increased, a phenotype similar to that observed upon transgenic overexpression of NLG1 (Dahlhaus et al., 2010). Moreover, application of a competitive PSD-95 peptide and neuroligin 1 C-terminal mutagenesis each specifically alter neuroligin 1 surface membrane expression and interfere with its internalization. Our data suggest the concept that synaptic plasticity regulates neuroligin turnover through active cytoskeleton transport.

Introduction

Neuroligins (NLGs) represent key postsynaptic proteins with a role in synapse instruction, maturation, and retrograde signaling (Südhof, 2008). They constitute a family of cell adhesion proteins that transsynaptically interact with presynaptic neurexins (NRXs) (Ichtchenko et al., 1995). The intracellular C-terminal PDZ binding domain of NLGs binds to several PDZ domain-containing scaffold proteins, which in turn couple to different ion channels, receptors, and molecules involved in signal transduction (Irie et al., 1997; Meyer et al., 2004). The transsynaptic NLG/NRX link is thought to be of key importance for synaptogenesis as well as the synaptic integrity at NLG/NRX-positive contacts (Scheiffele et al., 2000; Dean et al., 2003; Chih et al., 2005). Non-neuronal expression of NLGs induces formation of presynaptic specializations in contacting axons (Scheiffele et al., 2000; Dean et al., 2003; Chih et al., 2005). Furthermore, NLGs are thought to play a functional synaptic role by recruiting postsynaptic scaffolding proteins, receptors, and signaling molecules to nascent synapses (Südhof, 2008) and by modulating presynaptic release probability through retrograde signaling (Futai et al., 2007). Transient RNAi knockdown of NLG gene expression causes a reduction in synapse density (Chih et al., 2005), whereas neuroligin deficiency in NLG1/NLG2/NLG3 triple-knock-out mice impairs synaptic transmission but does not alter the density of synaptic contacts (Varoqueaux et al., 2006).

Postsynaptic density-95 (PSD-95) rapidly redistributes at excitatory spine synapses *in vivo* (Gray et al., 2006), is involved in synapse maturation, and directly binds to the NLG C-terminal PDZ binding motif (Irie et al., 1997). As a member of the MAGUK (membrane-associated guanylate kinase) family of postsynaptic density proteins, PSD-95 displays sequence homology to PSD-93, SAP97, and SAP102 (Fujita and Kurachi, 2000). In addition to interactions at the synapse, PSD-95 binds to the intracellular kinesin family protein KIF1Bα (Mok et al., 2002), an anterograde molecular motor that mediates cargo transport along microtubule tracks.

Received Feb. 18, 2010; revised July 30, 2010; accepted Aug. 4, 2010.

This work was supported by the University of Hamburg Medical School, Deutsche Forschungsgemeinschaft (DFG) Grants KN556/1-3 and FG885-KN556/4–1 and by the CHS Foundation to M.K. K.E.W. and E.L.F.H. were supported by National Institutes of Health Grant NS060698. We thank the following persons for kindly providing DNA constructs: R. Vallee for dynein intermediate chain 2B and dynamitin, R. Tsien for pmRFP, P. Washbourne and S. Vicini for GFP-NLG1, A. M. Craig for YFP-NLG1, S. Jamain for pcDNA3-myc-NLG1, and P. Scheiffele for mRFP-NRX1β. We thank W. Hirdes for help evaluating the mEPSCs. We thank the DFG-FG885 members for critical comments. The following authors performed and/or analyzed experimental data and contributed to the individual figures as follows: I.U.S.: 1*A–D*,*G*,*H*, 2*D–F*, 3*F–H*, *K*, *M*,*N*, 4*C*,*D*, 5*A–F*, 6*A–E*, 7*A–E*, S1*A*, *B*, S2*A–D*, S3*A–D*, S4*C*; B.B.: 2*A*, 3*A*, *E*, *I*, *J*,*L*, 4*A*, *B*, S3*B*, *D*, S4*D*; Y.P.: 3*K*, *M*, 5*C*, *D*, *F*, S3*B–D*; C.L.-S.: 5*C*,*D*, 7*C*,*D*, S3*D*; A.V.S.: 1*E*; F.B.: 3*D*; M.S.: 5*A*, *B*, S4*C*; D.S.: 1*F*; J.R.S.: 1*G*,*H*; M.K.: 2*A–D*, 3*A–C*, *M*, *N*, S3*A*, *D*; E.L.F.H. and K.E.W.: 4*A–D*, S4*A*, *B*; S.J.K.: S3*B–D*. E.L.F.H. and K.E.W. provided transgenic M21 mice. S.G.N.G. provided PSD-95 knock-out mouse brains. M.K. designed and coordinated the study. M.K. wrote the manuscript together with I.U.S.

*I.U.S. and B.B. contributed equally to this work.

Correspondence should be addressed to Prof. Dr. Matthias Kneussel, Center for Molecular Neurobiology (ZMNH), University of Hamburg Medical School, Falkenried 94, D-20251 Hamburg, Germany. E-mail: matthias.kneussel@zmnh.uni-hamburg.de.

DOI:10.1523/JNEUROSCI.0896-10.2010

 0270-6474/10/3012733-12$15.00/0

Long-distance transport (Caviston and Holzbaur, 2006) as well as endocytic/recycling processes between submembrane vesicle pools and the neuronal plasma membrane (Ehlers, 2000) uses actin- and microtubule-based motor protein complexes. Interestingly, microtubules have been recently found to enter dendritic spines in an activity-dependent manner (Hu et al., 2008; Jaworski et al., 2009). With respect to microtubule-based transport to, from, and between subcellular compartments, kinesin-family (KIF) proteins organize transport in anterograde directions (Hirokawa and Takemura, 2005), whereas cytoplasmic dynein represents the major motor for transport of molecular cargo in the retrograde direction (Vallee et al., 2004). Dynein is known to mediate processes such as retrograde transport of synaptic glycine receptors (GlyRs) (Maas et al., 2006) and neurotrophin receptors (Trks) (Heerssen et al., 2004), and participates in endocytosis pathways downstream of the sorting endosome (Traer et al., 2007).

Here, we asked whether NLGs that critically participate in a transsynaptic complex, which in turn tightly associates with presynaptic and postsynaptic membrane scaffolds, would at all undergo membrane turnover, independent of retracting the entire spine and/or synaptic contact. Furthermore, we aimed to understand whether dynamic NLGs use active cytoskeleton transport.

Materials and Methods

Cell culture, transfection, and immunochemistry

Primary hippocampal cultures were prepared from postnatal day 0 (P0) mice or rats as previously described (Loebrich et al., 2006; Maas et al., 2006). Neurons were transfected using a calcium phosphate protocol (Fuhrmann et al., 2002). Cells were fixed with 4% (w/v) paraformaldehyde (PFA)-PBS for 12 min, permeabilized with 0.2% (v/v) Triton X-100 for 4 min, and then blocked with 1% (w/v) bovine serum albumin (Applichem) in PBS for 30 min. Antibody staining was performed by incubation for 2 h with primary antibodies and 45 min for secondary antibodies in blocking buffer. GFP- and mRFP-fusion proteins were visualized by autofluorescence.

For immunohistochemistry, cryostat sections (10 μm) were permeabilized in 0.5% Triton X-100/PBS for 2 × 10 min. After brief washing with PBS and 60 min incubation in blocking solution (1% BSA, 10% goat serum in PBS), primary antibodies were applied overnight dissolved in 3% goat serum, 1% BSA, and 0.05% Triton X-100 in PBS. Secondary antibody incubation (in primary antibody solution) was performed for 1 h.

Chemical treatment designed to induce LTP and LTD

For chemical treatment designed to induce long-term potentiation (LTP) (Otmakhov et al., 2004; Oh et al., 2006; Kim et al., 2007), day *in vitro* 10 (DIV10) rat hippocampal neurons or acute slices (see below) were incubated for 20 min in Ringer solution (1 mM $MgCl_2$, 125 mM NaCl, 2.5 mM KCl, 2 mM $CaCl_2$, 33 mM D-glucose, 25 mM HEPES, pH 7.3) and 10 min in Ringer solution (125 mM NaCl, 2.5 mM KCl, 2 mM $CaCl_2$, 33 mM D-glucose, 25 mM HEPES, pH 7.3) supplemented with 50 μM forskolin and 0.1 μM rolipram (Tocris Bioscience). The solvent DMSO (Sigma, 1:1000) was used as a control. After PBS washing, a biotinylation assay was performed to analyze cell surface levels of NLG1/3 in cultured hippocampal neurons or acute slices. For chemical treatment designed to induce long-term depression (LTD) (Palmer et al., 1997; Huber et al., 2001; Snyder et al., 2001), DIV10 rat hippocampal neurons or acute slices were treated with 50 μM (*RS*)-3,5-dihydroxyphenylglycine (DHPG, Tocris Bioscience) for 5 min at 37°C. After washing with PBS, cells were incubated for 1 h at 37°C followed by surface biotinylation analysis to analyze cell surface levels of NLG1/3. To study chemical treatment designed to induce LTD in the presence of microtubule-depolymerizing agent, either 1 μM nocodazole (Tocris Bioscience) or DMSO (control) was applied simultaneously with 50 μM DHPG. In a second approach, 50 μM DHPG was applied alone for 5 min, followed by 1 μM nocodazole (Tocris Bioscience) application during the 1 h incubation time at 37°C. The effect of nocodazole alone was studied by adding 1 μM nocodazole (Tocris Bioscience) or DMSO (control) to cultured hippocampal neurons (DIV10) for 1 h. Subsequently, a biotinylation assay was performed.

Before biotinylation assays using potentiated or depressed acute tissue, 200 μm slices were cut from adult wild-type C57BL/6J hippocampi using a tissue chopper (McIlwain tissue chopper TC752). Slices were immediately transferred to a buffer, supplemented with 50 μM DHPG (Tocris Bioscience) or 50 μM forskolin and 0.1 μM rolipram (Tocris Bioscience) to induce either chemical LTD (cLTD) or chemical LTP (cLTP), respectively. Subsequently a biotinylation assay was performed as described below.

Surface biotinylation assay

A surface biotinylation assay was performed to assess the relative number of neuroligin molecules in the plasma membrane as a measure of Western blot signal intensities. For biotinylation of cell surface proteins, cells were washed with PBS, incubated with 1 mM biotinylation reagent (biotinamidohexanoic acid 3-sulfo-*N*-hydroxysuccinimide ester sodium salt, Sigma) for 20 min at 4°C and quenched twice with 100 mM glycine in HEPES buffer for 20 min at 4°C. Cells were harvested with PBS/1% Triton X-100, centrifuged at 1000 × *g* for 5 min, and then loaded on streptavidin beads (Dynabeads MyOne Streptavidin C1, Invitrogen) followed by an incubation period of 3 h at 4°C, with subsequent washing and resuspension in 4× SDS sample buffer.

Antibodies

The following antibodies were used for immunoprecipitation and Western blotting: anti-actin (1:2000, Sigma), anti-Arp1 (LaMonte et al., 2002), anti-pan-cadherin (1:2000, Abcam), anti-calbindin-D-28K (Sigma, 1:100), anti-dynamitin (IP1097) (LaMonte et al., 2002), anti-dynein intermediate chain (1:2000, Millipore Bioscience Research Reagents), anti-EEA1 (1:100, BD Bioscience), anti-Flag-M2 (1:250, Sigma), anti-GluR2 (1:50, Millipore), anti-KIF5C (1:2000, ABR), anti-Kinesin 1 (1:1000, Millipore Bioscience Research Reagents), anti-NLG1 (1:2000, Synaptic Systems), anti-NLG1/NLG3 (1:2000, Synaptic Systems), anti-N-cadherin (1:1000, Sigma), anti-nNOS (1:500, CST), anti-p22 (LaMonte et al., 2002), anti-p62 (LaMonte et al., 2002), anti-p150Glued (LaMonte et al., 2002), anti-PSD-95 (1:250, BD Bioscience), anti-PSD-95 (1:2000, ABR), anti-SAP97 (1:1000, ABR), mouse unspecific IgG (Sigma), and rabbit unspecific IgG (Sigma). The following antibodies were used for immunofluorescence: anti-dynein heavy chain (1:50, Santa Cruz Biotechnology), anti-myc (1:50, Sigma), anti-PSD-95 (1:100, ABR), anti-PSD-95 (1:200, Cell Signaling Technology), and anti-synaptophysin (1:100, Santa Cruz Biotechnology). The following secondary antibodies were used: HRP-conjugated anti-mouse or anti-rabbit (both 1:10,000, Dianova) and CY2-, CY3-, or CY5-conjugated donkey anti-goat, anti-mouse, or anti-rabbit (all 1:500, Dianova).

Constructs

The following constructs have been previously described: GFP-NLG1 (Fu et al., 2003; Barrow et al., 2009), YFP-NLG1 (Graf et al., 2004), and dynamitin-EGFP (Palazzo et al., 2001). To generate GFP-PSD-95, the PSD-95 cDNA was subcloned as EcoRI-SalI fragment into pEGFP-N2 (BD Bioscience). The plasmid mRFP-DIC was generated by subcloning the DIC2B cDNA as BglII/KpnI fragment into pmRFP1. To generate GFP-PSD-95 (256–398), a corresponding PCR product was subcloned as EcoRI-SalI fragment into pEGFP-C2 (BD Bioscience). For myc-NLG1ΔC-term., lacking the C-terminal 6 aa (HSTTRV) that correspond to the PDZ binding motif, a PCR product was subcloned as HindIII-XbaI fragment into pcDNA3 (Invitrogen).

Time-lapse imaging

Time-lapse imaging to analyze particle mobility of GFP-NLG1, GFP-PSD-95, and mRFP-DIC in cultured hippocampal neurons was performed as described previously (Maas et al., 2006). In brief, images were taken with an inverted fluorescent microscope Axiovert 200M (Zeiss) combined with a charge-coupled device camera (SPOT RT-SE, Sony),

equipped with a high-speed filter wheel for sequential image acquisition. Image acquisition intervals from 5 to 60 s were used.

Mass spectrometry

Bands were isolated from colloidal Coomassie-stained protein gels. Proteins were reduced with 10 mM dithiothreitol (DTT) and cysteine residues modified with 55 mM iodoacetamide before overnight in-gel trypsin digestion at 37°C (5 ng/μl trypsin in 50 mM NH_4HCO_3). Gel pieces were subsequently extracted in 50% acetonitrile/5% formic acid, vacuum concentrated, and redissolved in 0.1% trifluoroacetic acid (TFA)/water. For measurements, samples were applied by the dried droplet method using α-cyano-4-hydroxycinnamic acid (ACCA) as matrix. Mass spectra were acquired on a REFLEX IV (Bruker). For data base analysis, the Mascot peptide mass fingerprint search algorithm (Matrix Science) was applied.

Coimmunoprecipitation

Brains of eight P10 rats were dissected in ice-cold PBS and homogenized in IM-Ac buffer (20 mM HEPES, 100 mM K-acetate, 40 mM KCl, 5 mM EGTA, and 5 mM $MgCl_2$, pH 7.2) with freshly added protease inhibitor cocktail (Roche), 5 mM DTT, and 2 mM magnesium-ATP. Homogenates were clarified by centrifugation at 1000 × *g* for 10 min and the postnuclear supernatant was used for the following steps. First, the supernatant was centrifuged at 10,000 × *g* for 10 min to pellet large membrane organelles (P2). The remaining supernatant was further centrifuged at 100,000 × *g* to collect small membrane organelles (P3). After coupling 4 μg of antibodies to magnetic Protein G Dynabeads (Invitrogen) in IP buffer (50 mM Tris, pH 7.5; 150 mM NaCl; 5 mM $MgCl_2$; 0.5% Triton X-100), extracts from P3 fractions were incubated in IP buffer containing 0.5% Triton X-100 together with the beads for 4 h, followed by extensive washing steps with IP buffer containing 0.5% Triton X-100. Bound proteins were eluted by boiling in SDS-containing sample buffer and examined by Western blotting (Maas et al., 2006).

Imaging

Cells at the microscope stage were kept in HEPES buffer (10 mM HEPES, 135 mM NaCl, 5 mM KCl, 2 mM $CaCl_2$, 2 mM $MgCl_2$, 15 mM glucose) and temperature (37°C) and CO_2 controlled (Maas et al., 2006). For FM-dye labeling of active synapses, cells were exposed to 50 μM DL-APV and 15 μM FM4-64 for 1 min in 31.5 mM NaCl, 90 mM KCl, 5 mM HEPES, 1 mM $MgCl_2$, 2 mM $CaCl_2$, and 30 mM glucose. For FM-dye imaging, cells were kept in HEPES buffer containing 50 μM DL-APV and 10 μM DNQX (Maas et al., 2006). Fluorescence colocalization studies were performed with either an inverted Leica TCS-SP2 (Leica) or an upright Olympus FluoView TMFV1000 (Olympus) laser scanning confocal microscope using either 40× or 63× objectives. For simultaneous multichannel fluorescence, images were taken in a sequential recording mode.

Preparation of postsynaptic densities

Synaptosomes were prepared according to a previous protocol (Rogers et al., 1991). In brief, tissues were homogenized in a glass polymer homogenizer using 9 volumes of ice-cold dissection buffer (50 mM Tris-acetate, pH 7.0, 10% sucrose, 5 mM EDTA) containing protease inhibitor cocktail (Roche). Homogenates were centrifuged at 800 × *g* for 20 min. Resulting supernatants were centrifuged at 16,000 × *g* for 30 min. Resulting pellets were rehomogenized in 20 mM HEPES buffer, pH 7.4, and centrifuged at 16,000 × *g* for 15 min followed by resuspension in 5 volumes of lysis buffer (5 mM Tris-acetate, pH 8.1 including protease inhibitors). After incubation on ice for 45 min, homogenates were supplemented to get a final concentration of 34% (w/w) sucrose and 5 mM Tris-acetate, pH 7.4. Homogenate was overlaid with an equal volume of 28.5% (w/w) sucrose/Tris-acetate and another equal volume of 10% (w/w) sucrose/Tris-acetate, followed by gradient centrifugation at 60,000 × *g* for 2 h. Bands at the 28.5% and 34% interface were collected, diluted in 10% (w/w) sucrose/Tris-acetate, and pelleted by centrifugation at 48,000 × *g* for 30 min. The resulting pellet containing synaptosomes was resuspended in Tris-acetate buffer. For preparation of PSDs, the remaining pellet was homogenized using a glass homogenizer. An equal amount of 3% (v/v) Triton X-100 was added for 30 min with occasional mixing. Samples were layered on top of 28.5% (w/w) sucrose/Tris-acetate and centrifuged at 105,000 × *g* for 1 h. The resulting pellet containing postsynaptic densities was resuspended in Tris-acetate buffer.

Electron microscopy

Mice were anesthetized and perfused with 4% PFA and 3% glutaraldehyde in PBS. One-hundred-micrometer vibratome sections of the cerebellum were cut. After fixation with 1% OsO_4, the sections were dehydrated in an ascending series of ethanol and embedded in Epon (Carl Roth). Ultrathin sections were examined with a Zeiss EM 902 electron microscope. Approximately 100 micrographs were randomly taken from sections of each animal at a magnification of 20,000× in the outer third of the molecular layer with a Megaview III camera and the iTEM (SIS) software.

The analysis of PSD length and spine head area size was blindly performed using Meta Imaging Series 7.1/MetaMorph Offline and analySIS 3.0. For measurements of synapse number the results were manually controlled.

Internalization assay

Cultured hippocampal neurons were transfected with plasmids encoding wt or mutant myc-NLG1ΔC-term., with equal amounts of plasmid encoding EGFP, Dynamitin-EGFP, or GFP-PSD-95 (256–398). Twenty-four hours after transfection, cells were incubated with anti-myc for 1 h at 4°C. Upon removal of excess antibody, cells were incubated at 37°C for a 2 h period to allow endocytosis to occur. After this, cell surface myc-NLG1 was detected with Cy5-conjugated secondary antibody (blue signal) in the absence of permeabilization at 4°C. Cells were subsequently fixed in 4% PFA/4% sucrose for 10 min and permeabilized with 0.25% Triton X-100/PBS for 5 min. After blocking with 1% BSA/PBS for 30 min, internalized primary antibodies were detected with Cy3-conjugated secondary antibody (red signal). Cells were washed twice in PBS and mounted in Aqua Poly Mount (Polysciences). As a negative control, 350 mM sucrose was used during the whole procedure to block endocytosis. Internalization of GluR2 was performed as described above; however, instead of anti-myc, an anti-GluR2 antibody was used to visualize internalized GluR2.

Electrophysiology

Cultures. Experiments were done on hippocampal neurons (DIV10–12) with the whole-cell configuration of the patch-clamp technique (Hamill et al., 1981; Goddard et al., 2007). For stimulation and data acquisition the Pulse 8.65 software (HEKA) in combination with an EPC-9 patch-clamp amplifier (HEKA) was used. Data were low-pass filtered at 2.9 kHz. Experiments were done at room temperature (21–23°C). Pipettes were made from borosilicate glass capillaries and coated with Sigmacote. When filled with intracellular solution the pipette resistance was 3.0–4.0 MΩ. Data were analyzed with PulseFit (HEKA), Mini Analysis (Synaptosoft), Igor (Wavemetrics), and Excel (Microsoft). The extracellular solution contained the following: 143 mM NaCl, 5 mM KCl, 0.8 mM $MgCl_2$, 1 mM $CaCl_2$, 10 mM HEPES, 5 mM glucose, 0.5 μM TTX, and 20 μM bicuculline, pH adjusted to 7.3 with NaOH. In some experiments, the extracellular solution contained in addition CNQX (20 μM) and APV (20 μM) which completely blocked mEPSCs. The pipette solution contained the following: 120 mM K-gluconate, 8 mM NaCl, 2 mM $MgCl_2$, 0.5 mM $CaCl_2$, 5 mM EGTA, 10 mM HEPES, 14 mM phosphocreatine, 2 mM magnesium-ATP, and 0.3 mM sodium-GTP, pH adjusted to 7.3 with KOH. Neurons successfully transfected with dynamitin-EGFP were detected by their GFP fluorescence. Measurements were made between 16 and 24 h after transfection. Except where indicated, all chemicals were purchased from Sigma.

Slices. Sagittal slices of the hippocampal formation were prepared from male C57BL/6N mice (P29–P30) in accordance with national and institutional guidelines. The animals were anesthetized with isoflurane and decapitated. Their brains were quickly removed and submerged in ice-cold ACSF containing the following: 87 mM NaCl, 50 mM sucrose, 26 mM $NaHCO_3$, 10 mM glucose, 2.5 mM KCl, 1.25 mM NaH_2PO_4, 3 mM $MgCl_2$, and 0.5 mM $CaCl_2$, equilibrated with 95% O_2 and 5% CO_2, pH 7.4. Tissue blocks containing the hippocampus were mounted on a vibratome (VT1200S, Leica Microsystems) in a submerged chamber and cut at 300 μm thickness. After an incubation period of 30 min at 35°C, the slices

were stored at room temperature and kept for 1–5 h before being transferred to the recording chamber. Field recordings were performed at room temperature. The slices were viewed with a fixed stage upright microscope (Olympus) and perfused at a rate of 5 ml/min with ACSF containing the following: 119 mM NaCl, 26 mM $NaHCO_3$, 10 mM glucose, 2.5 mM KCl, 2.5 mM $CaCl_2$, 1.3 mM $MgCl_2$, and 1 mM NaH_2PO_4. For chemical LTP induction, slices were perfused for 10 min with ACSF containing the following: 119 mM NaCl, 26 mM $NaHCO_3$, 10 mM glucose, 2.5 mM KCl, 2.5 mM $CaCl_2$, 1 mM NaH_2PO_4, 50 μM forskolin, and 0.1 μM rolipram. For chemical LTD induction, slices were perfused for 5 min with 50 μM DHPG. The recording and stimulation electrodes (thin-walled borosilicate glass capillaries, Harvard Apparatus) had diameters of ~7 μm and ~10 μm, respectively. They were filled with ACSF and placed in stratum radiatum of area CA1. Field responses were evoked by electrical stimulation (100 μs every 1 min) using a stimulus isolator (ISO-flex, A.M.P.I.). Prior each experiment, the stimulus strength was adjusted to produce an fEPSP amplitude ~50% of that which elicited a population spike. Input signals were amplified using an Axopatch 700B Amplifier (Molecular Devices). Data were acquired using a BNC-2090 interface board (National Instruments) and IGOR Pro 4 software (Wavemetrics) (digitized at 5 kHz and low-pass filtered at 2 kHz). All electrophysiological data were analyzed using IGOR Pro 4. The slope of each individual fEPSP was calculated from its 20–80% rise time. Average values are expressed as mean ± SEM.

Sucrose gradient

Fractionation of brain homogenates of wild-type and transgenic M21 mice was performed as previously described (LaMonte et al., 2002).

Quantitative data analysis

For evaluation of relative Western blot signal intensities, films were scanned with a resolution of 600 dpi and signals subsequently analyzed using the ImageJ, version 1.38 analysis software (National Institutes of Health). Signal intensities were normalized, as compared to loading control signals. Quantitative data display average values from independent experiments. For colocalization studies, confocal images from multiple individual cells were obtained using identical photomultiplier values throughout individual coverslips. TIFF files were eventually contrast and/or brightness adjusted using Adobe Photoshop CS2, keeping identical input levels for each channel throughout all parallel images. For analysis of mobile puncta, images were acquired using the MetaVue 6.2r6 software connected to the digital camera. Image stacks were subsequently loaded into MetaMorph 7.1 and mobile puncta from unprocessed images were followed throughout individual frames. To compensate strong light intensities in cell bodies, brightness was eventually reduced to track mobile puncta in somata. Due to the inability of MetaMorph

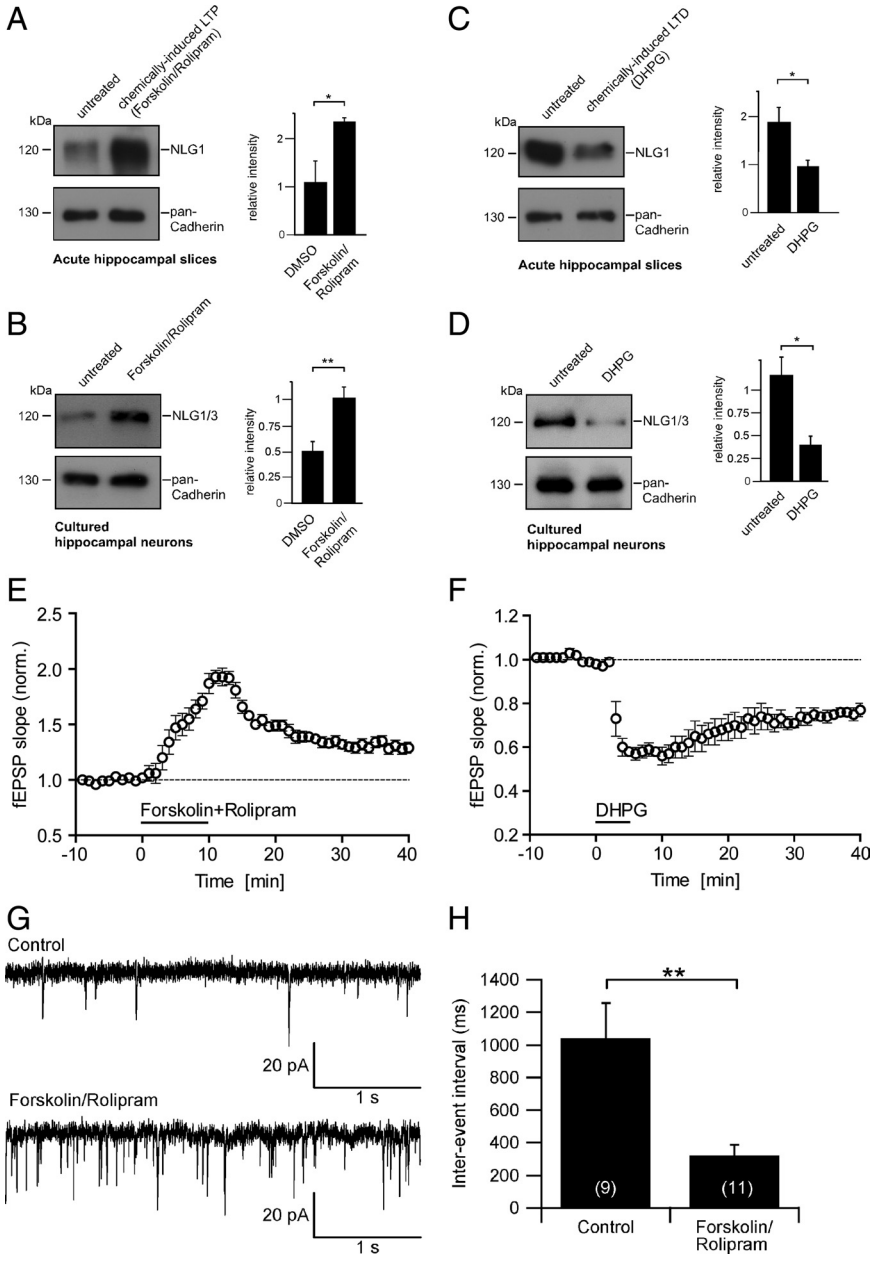

Figure 1. Altered NLG1 surface membrane levels upon application of chemical treatment designed to induce LTP or LTD, respectively. ***A***, ***B***, Chemical treatment designed to induce LTP significantly increases NLG1/3 at neuronal surface membranes. ***A***, Surface biotinylation analysis of acute hippocampal slices detected against NLG1 and pan-cadherin (loading control). ***B***, Neuronal surface biotinylation analysis of NLG1/3 and pan-cadherin (loading control) in cultured hippocampal neurons. ***C***, ***D***, Chemical treatment designed to induce LTD significantly reduces NLG1/3 from neuronal surface membranes. ***C***, Surface biotinylation analysis of acute hippocampal slices detected against NLG1 and pan-cadherin (loading control). ***D***, Neuronal surface biotinylation analysis of NLG1/3 and pan-cadherin (loading control) in cultured hippocampal neurons. Values reflect relative Western blot signal intensities of surface membrane NLG1/3 protein levels, analyzed using the ImageJ software. Error bars represent the SEM. $*p < 0.05$; $**p < 0.01$. ***E***, ***F***, Chemical LTP or chemical LTD induction in acute slices of P30 C57BL/6N mice causes a long-lasting increase or depression of fEPSPs, respectively. ***E***, Chemical LTP induction by treatment with forskolin and rolipram led to a long-term increase of fEPSPs by 30% (average of the normalized fEPSP slopes in the last 5 min of recording: 1.29 ± 0.05, $n = 5$). ***F***, Chemical LTD induction by DHPG treatment caused long-term depression of fEPSPs by 32% (average of the normalized fEPSP slopes in the last 5 min of recording: 0.76 ± 0.03, $n = 4$). ***G***, Examples showing recordings of spontaneous mEPSCs from a control cultured hippocampal neuron (upper panel) and a cultured neuron treated with forskolin/rolipram (lower panel). ***H***, Mean ± SEM of interevent intervals of control (DMSO treatment) and forskolin/rolipram-treated neurons; the graph shows a very significant difference between the two means (control: 1041.12 ± 216.29 ms, $n = 9$; forskolin/rolipram: 321.22 ± 65.63 ms, $n = 11$; $p < 0.01$). Forskolin/rolipram treatment induces a drastic increase in synaptic activity. The mean values of mEPSC amplitudes of the two groups of neurons were slightly different; however, this difference was not statistically significant (control: 14.4 ± 1.2 pA; forskolin/rolipram: 17.0 ± 2.0 pA; $p = 0.296$). Error bars represent the SEM. $**p < 0.01$.

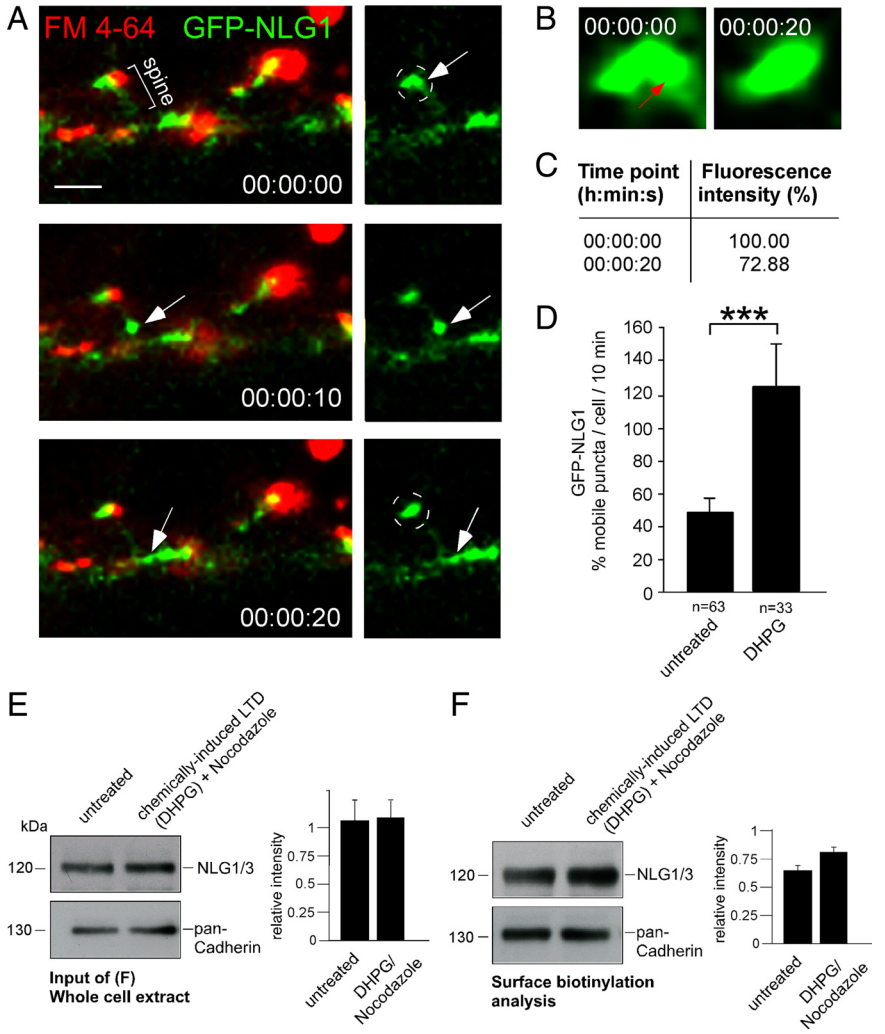

Figure 2. NLG1 leaves dendritic spine heads and LTD-induced NLG internalization requires intact microtubules. ***A***, A GFP-NLG1 particle (green, white arrows) leaves a synapse. Active presynaptic terminals are represented through FM4-64 (red). Scale bar, 1.5 μm. The spine head (white circles) is magnified in ***B***. ***B***, ***C***, Fluorescence intensities of white circles in ***A***. Red arrow, Particle that just starts to emerge from the postsynaptic compartment. ***D***, Chemical treatment designed to induce LTD through DHPG significantly increases the number of mobile GFP-NLG1 particles in cultured hippocampal neurons. ***E***, ***F***, In the presence of the microtubule-depolymerizing agent nocodazole, chemical treatment designed to induce LTD does not reduce NLG1/3 from neuronal surface membranes. ($n = 4$ experiments) (compare with Fig. 1*C*,*D*). ***E***, Whole-cell extract detected against NLG1/3 (input). Pan-cadherin detection, Loading control. ***F***, Neuronal surface biotinylation analysis of NLG1/3. Pan-cadherin, Loading control. Values reflect relative Western blot signal intensities of surface membrane NLG1/3 protein levels, analyzed using the ImageJ software. Error bars represent the SEM. $^{***}p < 0.001$.

to reliably track crossing particles, the program's "Track Objects" function was excluded and mobile particles were instead manually tracked per mouse click throughout each individual frame. Direction of movement (anterograde vs retrograde) was assessed by comparing the position of each particle between the first and last frame of each stack. Due to alternate mobility of individual puncta, average maximal velocities between two acquisition frames (instantaneous velocity) were assessed for maximal comparison. Fluorescence intensity measurements (arbitrary pixel units) were performed using the "Region Statistics" function within MetaMorph. Identical regions of interests (ROIs) were defined, covering signals of interest throughout multiple image acquisition frames. Average intensities within each ROI are compared. For analysis of pulse-chase internalization values, two subsequent measurements were performed using MetaMorph 7.1. First, colocalization values of blue and red signals (magenta) were assessed. In a second step, intracellular myc-NLG1 signals from the same cell (red) were measured. To achieve a corrected value for internalization rates, overlapping signals (magenta) were subsequently subtracted from red signals. Statistical analysis was performed with Microsoft Excel. The Student's *t* test was used to assess statistical significance. $^{*}p < 0.05$; $^{**}p < 0.01$; $^{***}p < 0.001$.

Results

Altered neuroligin 1/3 surface membrane levels upon chemical treatment designed to induce LTP or LTD

Since postsynaptic NLG1 connects presynaptic terminals and postsynaptic spines through a transsynaptic interaction with NRX1β (Südhof, 2008), we asked whether a factor that critically participates in an intercellular connection of this kind would at all be subject to protein exchange at synapses. To address this, we applied chemical treatment designed to induce LTP in acute hippocampal slices and cultured hippocampal neurons through application of a forskolin/rolipram protocol (Otmakhov et al., 2004; Oh et al., 2006; Kim et al., 2007). Notably, surface biotinylation analysis revealed that NLG1/3 levels at the neuronal plasma membrane were significantly increased upon a persistent enhancement in synaptic strength (slices: untreated 1.09 ± 0.44, $n = 3$; forskolin/rolipram 2.36 ± 0.10, $n = 3$, $p < 0.05$; cultures: untreated 0.51 ± 0.10, $n = 6$; forskolin/rolipram 1.02 ± 0.11, $n = 6$; $p < 0.01$) (Fig. 1*A*,*B*). This effect was specific and not due to changes in NLG gene expression as revealed from analysis of whole-cell extracts, in comparison to a loading control (supplemental Fig. S1*A*, available at www.jneurosci.org as supplemental material). Control electrophysiological recordings confirmed that forskolin/rolipram induce cLTP at Schaffer collateral–CA1 synapses, leading to a long-lasting increase of fEPSPs by 30% (Fig. 1*E*). Moreover, we induced cLTP in cultured hippocampal neurons, which resulted in a strong increase in synaptic activity (Fig. 1*G*,*H*).

In contrast, application of chemical treatment designed to induce LTD through the mGluR agonist DHPG caused long-term depression of fEPSPs by 32% in acute hippocampal slices (Fig. 1*F*) (Palmer et al., 1997; Huber et al., 2001), and is known to decrease synaptic activity in cultured hippocampal neurons (Snyder et al., 2001). In the analysis of neuronal NLG1 surface membrane levels, this treatment caused significant effects in both acute slices and cultured neurons leading to NLG1 decrease at neuronal plasma membranes (slices: untreated 1.89 ± 0.31, $n = 3$; DHPG 0.95 ± 0.15, $n = 3$, $p < 0.05$; cultures: untreated 1.14 ± 0.30, $n = 5$; DHPG 0.39 ± 0.08, $n = 5$; $p < 0.05$) (Fig. 1*C*,*D*). Also under these conditions, total NLG1/3 levels remained unchanged in whole-cell extracts, indicating that NLG proteolysis or a decrease in NLG1/3 gene expression was not an issue in this respect (supplemental Fig. S1*B*, available at www.jneurosci.org as supplemental material).

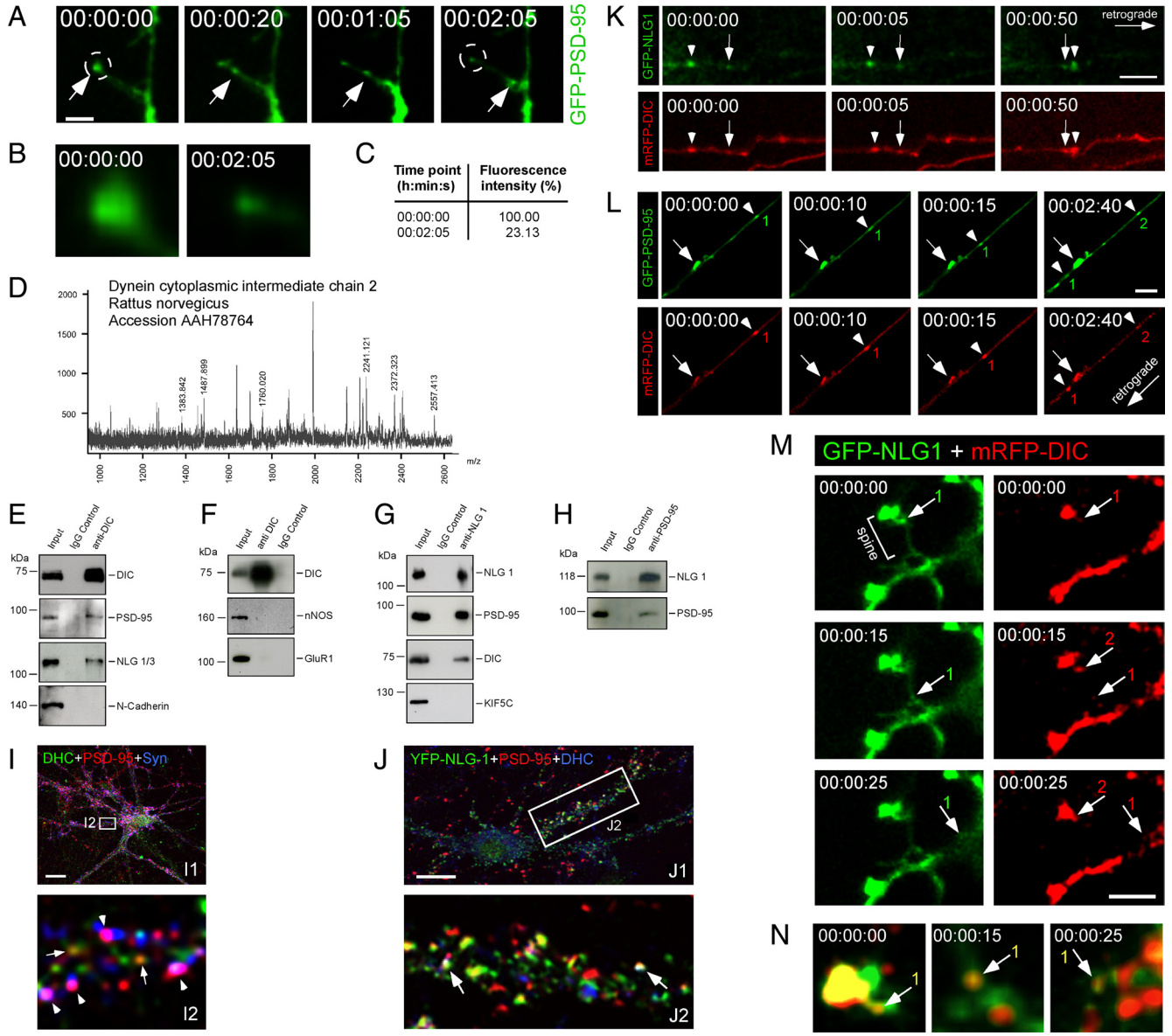

Figure 3. *In vitro* binding, colocalization, and cotransport of NLG1, PSD-95, and dynein. ***A***, A GFP-PSD-95 particle leaves a dendritic spine head over time. Scale bar, 0.2 μm. ***B***, ***C***, Fluorescence intensities of white circles in ***A***. ***C***, The reduced signal intensity indicates removal of fluorescent material. Controls were performed to rule out that these changes refer to bleaching (not shown). ***D***, Mass spectrometry identifies DIC as a PSD-95 binding partner. ***E–H***, Co-IPs from P10 rat brain vesicle-enriched fractions (P3). DIC-specific antibodies coprecipitate PSD-95 and NLG1/3, but not N-cadherin, nNOS, or GluR1. NLG1-specific antibodies coprecipitate PSD-95 and DIC, but not the motor KIF5C. PSD-95-specific antibodies coprecipitate intracellular nonsynaptic NLG1 (P3 lysate). ***I***, Immunocytochemical analysis of DIV10–14 cultured hippocampal neurons. Dynein heavy chain (DHC) and PSD-95 colocalize at nonsynaptic, synaptophysin (Syn)-negative sites (yellow, arrows). The majority of PSD-95 is synaptic (magenta, arrowheads; supplemental Fig. S3*B*, available at www.jneurosci.org as supplemental material). ***J***, Triple colocalized puncta of YFP-NLG1, PSD-95, and DHC are found in neurites (white, arrows; supplemental Fig. S3*C*, available at www.jneurosci.org as supplemental material). ***K***, Retrograde neuronal cotransport of GFP-NLG1 and mRFP-DIC particles in neurites over time. ***L***, Retrograde neuronal cotransport of GFP-PSD-95 and mRFP-DIC particles in neurites over time. Scale bars (***K***, ***L***), 2.5 μm. ***M***, ***N***, Time-lapse video microscopy on cultured hippocampal DIV 13 neurons, coexpressing GFP-NLG1 (green) and mRFP-DIC (red). The merged particle (indicated as 1) is magnified in ***N*** (yellow) for each time point. It moves from the spine head through the neck of the spine and within the parent dendrite further to the right, indicating that dynein-dependent transport is involved in this process. A second particle appears in the red channel at time point 15 s that remains stable over the rest of the movie.

Intact microtubules are required for LTD-induced removal of neuroligin 1/3 from neuronal surface membranes

To analyze whether these results reflected spine formation/retraction or protein exchange of NLG particles, we performed time-lapse video microscopy with a fluorescent GFP-fusion protein of NLG1. This fusion protein has been previously described (Fu et al., 2003; Barrow et al., 2009), localizes to dendritic spines (supplemental Fig. S3*A*, available at www.jneurosci.org as supplemental material) and colocalizes with its binding partners PSD-95 and postsynaptic NRX1β (Taniguchi et al., 2007) (supplemental Fig. S3*A*, available at www.jneurosci.org as supplemental material).

Live-cell imaging on DIV12–14 cultured hippocampal neurons revealed individual particles that entered (not shown) and left (Fig. 2*A–C*) dendritic protrusions over time. However, as particle delivery could just reflect newly formed growing contacts, we focused on retrogradely moving particles that left spine heads, which harbor the postsynaptic site of excitatory synapses. We found that GFP-NLG1 moved in both directions through neurites, displaying alternate movement and pausing with a max-

imal velocity of 0.11 ± 0.02 μm/s ($n = 19$ particles, 3 experiments) (supplemental Fig. S3*D*, available at www.jneurosci.org as supplemental material). Individual GFP-NLG1 particles left the spine head and moved down its neck toward the underlying parent dendrite (Fig. 2*A*). In parallel, active presynaptic terminals were labeled with the red fluorescent dye FM4-64, to ensure that the analyzed spine compartments were innervated and represented functional synapses (Fig. 2*A*). Fluorescence intensity analysis (Fig. 2*B*) confirmed the loss of fluorescent molecules after particle egression (white circles in Fig. 2*A*,*C*) and proved that the majority of GFP-NLG1 signals remained at the spine synapse that was not subject to spine retraction (Fig. 2*A*, lower image).

Consistent with decreased NLG1 surface membrane levels upon DHPG treatment designed to induce LTD (Fig. 1*C*,*D*), DHPG also caused a highly significant increase in the number of GFP-NLG1 particles that were mobile over the time period analyzed (untreated: 48.0 ± 9.0%, $n = 63$ movies, 9 experiments; DHPG: 124.0 ± 25.0%, $n = 33$ movies, 5 experiments, $p < 0.001$) (Fig. 2*D*), suggesting that changes in synaptic strength can alter NLG1 intracellular transport. We therefore asked whether intact microtubules, known to enter dendritic spines in an activity-dependent manner (Hu et al., 2008; Jaworski et al., 2009) and to mediate long-distance transport (Hirokawa and Takemura, 2005), would be a prerequisite for NLG internalization upon DHPG-induced LTD induction. Indeed, combination of DHPG with the microtubule-depolymerizing agent nocodazole prevented the formerly identified (compare with Fig. 1*C*,*D*) reduction of NLG1/3 signals from neuronal surfaces [inputs: untreated: 1.08 ± 0.19, $n = 4$; DHPG+nocodazole: 1.10 ± 0.17, $n = 4$ (Fig. 2*E*); biotinylation analysis: untreated: 0.65 ± 0.06, $n = 4$; DHPG+nocodazole: 0.82 ± 0.05, $n = 4$ (Fig. 2*F*; supplemental Fig. S2, available at www.jneurosci.org as supplemental material)], a finding that suggested that active cytoskeleton transport might be an underlying mechanism for induced NLG turnover.

Association and colocalization of neuroligin 1 with components of the dynein motor complex

Different microtubule transport complexes in neurons use postsynaptic anchoring proteins to connect transmembrane cargo to molecular motors (Setou et al., 2000, 2002; Maas et al., 2006). We therefore asked whether the NLG1 C-terminal binding partner PSD-95 (Irie et al., 1997) could link NLG1 to a motor involved in active cytoskeleton transport. Mobile GFP-PSD-95 fluorescent particles were also found to enter (not shown) and leave (Fig. 3*A*) spine protrusions in retrograde directions. They moved with maximal velocities of 0.31 ± 0.06 μm/s ($n = 15$ particles, 3 experiments) (supplemental Fig. S3*D*, available at www.jneurosci.org as supplemental material), and fluorescence intensity analysis consistently revealed decreasing intensity values after the egression of subparticles (Fig. 3*B*,*C*). In subsequent co-IP experiments from P10 rat brain vesicle-enriched fractions (P3-lysate) using PSD-95-specific antibodies, followed by mass spectrometry (MS), we indeed identified a dynein intermediate chain (DIC, GenBank protein accession number AAH78764) as being part of a PSD-95 complex (Fig. 3*D*), suggesting that PSD-95 might associate with dynein motors in transit. Consistent with this result upon MS analysis, immunoprecipitation with DIC-specific antibodies from vesicle-enriched lysates led to co-IP of both PSD-95 and NLG1/3, whereas the unrelated protein N-cadherin was not part of the putative transport complex (Fig. 3*E*). Also the postsynaptic submembrane and transmembrane

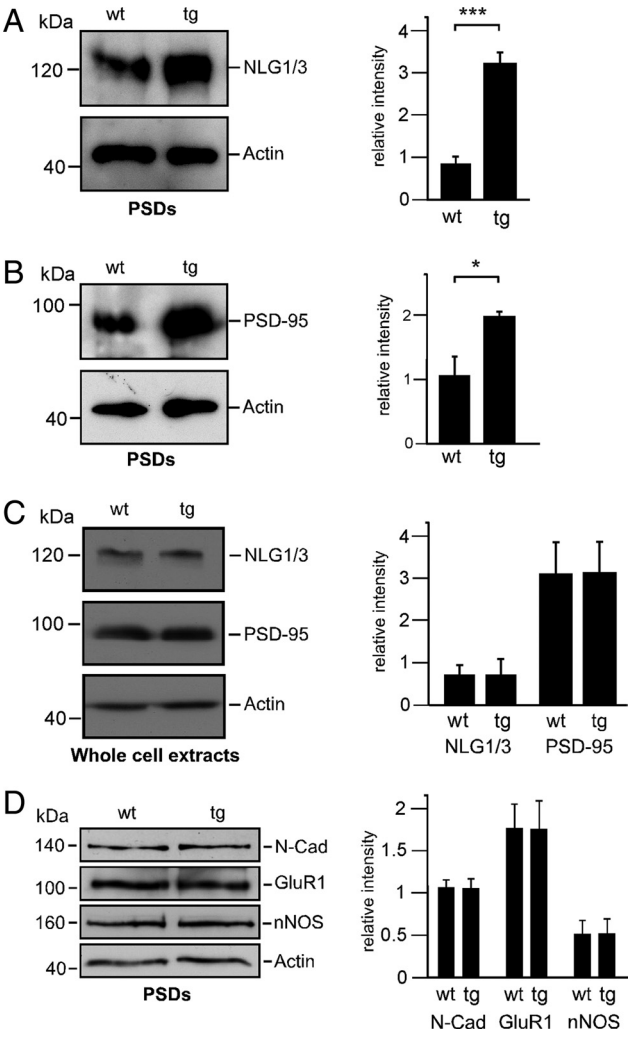

Figure 4. Increased protein levels at PSDs upon functional dynein inhibition. Analysis of brains derived from wt mice or tg mice that overexpress dynamitin under the postnatal Thy-1 promoter is shown. ***A***, ***B***, Quantitative evaluation of protein levels at PSDs. NLG1/3 (***A***) and PSD-95 (***B***) are significantly enriched at PSDs in the absence of retrograde transport. Actin, Loading control. ***C***, Control analysis of whole-cell extracts confirming that the identified changes in ***A*** and ***B*** are due to redistributions of the proteins analyzed and do not represent an overall change in gene expression. Actin, Loading control. ***D***, Control evaluation of protein levels at PSDs. Other postsynaptic transmembrane (N-cadherin, GluR1) and submembrane (nNOS) proteins remain unaltered under the same conditions as shown in ***A*** and ***B***. Values reflect relative Western blot signal intensities, analyzed using the ImageJ software. Error bars represent the SEM. $*p < 0.05$; $***p < 0.001$.

proteins nNOS and the AMPA receptor subunit GluR1, respectively, were not subject to coprecipitation (Fig. 3*F*), indicating specificity of the above results. Reciprocal experiments with an NLG1-specific antibody (Song et al., 1999) consistently revealed co-IP of both PSD-95 and DIC, but not KIF5C, an unrelated microtubule motor detected as a control (Fig. 3*G*). Finally, a control confirmed that the reported interaction of PSD-95 and NLG (Irie et al., 1997) occurs not only at synaptic membranes, but also at intracellular vesicle-enriched fractions (Fig. 3*H*). Immunocytochemical analysis consistently identified overlapping particles of the dynein subunit DHC and PSD-95 at nonsynaptic, putatively intracellular, positions (Fig. 3*I*, arrows; supplemental Fig. S3*B*, available at www.jneurosci.org as supplemental material) and revealed triple colocalization of YFP-NLG1, PSD-95, and DIC in neurites (Fig. 3*J*, arrows; supplemental Fig. S3*C*, available at www.jneurosci.org as supplemental material).

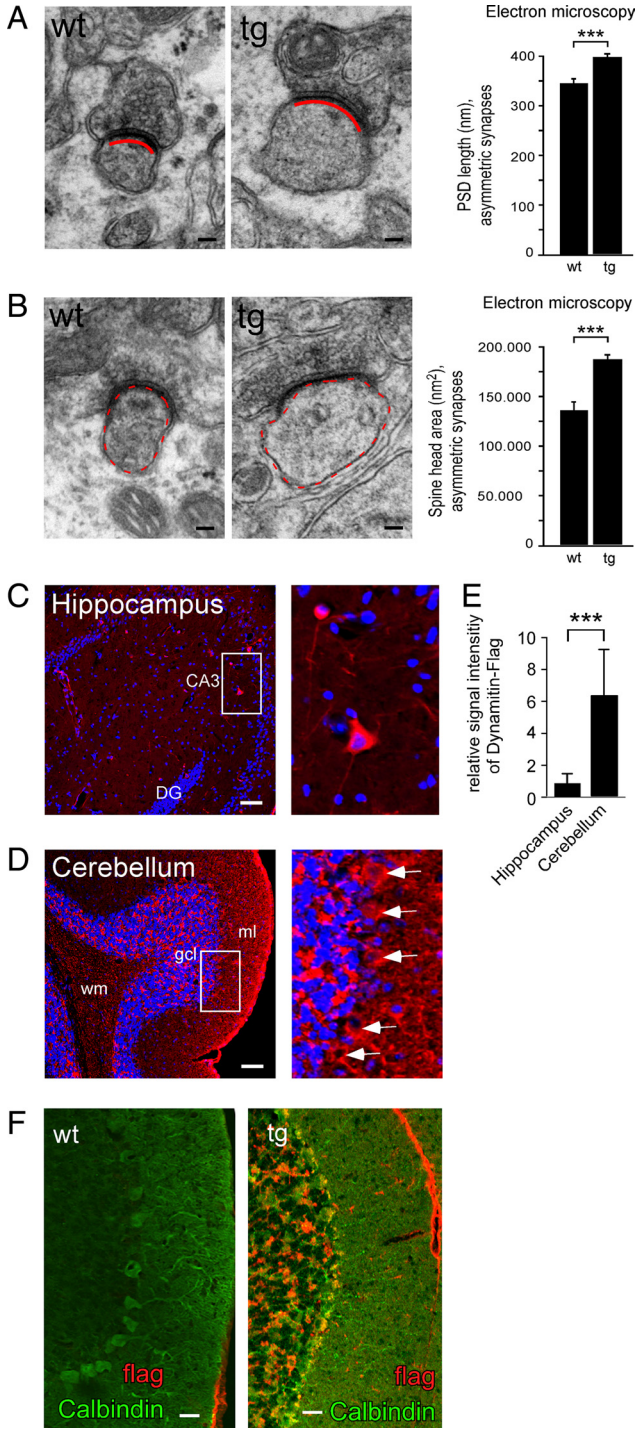

Figure 5. Increased PSD lengths and spine head areas upon inhibition of dynein-mediated retrograde transport *in vivo*. Electron microscopy analysis of parallel fiber–Purkinje cell synapses derived from cerebellar slices of adult wt and tg mice (age: 12 months) that overexpress dynamitin under the postnatal Thy-1 promoter (LaMonte et al., 2002) is shown. Purkinje cells express the flag-tag representing the transgene (compare with ***D*** and ***F***). ***A***, PSD lengths at asymmetric synapses are significantly increased in tissue derived from tg mice, represented through dynein inhibition, as compared to tissue derived from wt mice. PSDs are underlined in red ($n = 3$ animals per genotype). ***B***, Spine head areas are significantly increased in tissue derived from tg mice, represented through dynein inhibition, as compared to tissue derived from wt mice. Areas used for analysis are highlighted through dashed lines in red. ($n = 3$ animals per genotype). Scale bars, 100 nm. Note that the single transgenic overexpression of NLG1 causes similar changes (Dahlhaus et al., 2010). Error bars represent the SEM. ***$p < 0.001$. ***C***, ***D***, Immunohistochemical detection of dynamitin-flag (red) in hippocampus (***C***) and cerebellum (***D***) of transgenic M21 mice. No obvious clinical symptoms have been identified or

It was not in the focus of this study to map individual binding sites for direct interactions, and it is possible that additional accessory or linker proteins may be involved in the actual complex. However if the above *in vitro* binding and colocalization data reflected a functional dynein-dependent motor-cargo complex that includes NLG1 and PSD-95, both factors should display neuronal comigration with a dynein motor subunit. Application of time-lapse video microscopy on DIV12–14 neurons accordingly displayed cotransport of both GFP-NLG1 ($n = 10$ particles, 3 experiments) (Fig. 3*K*,*M*,*N*; supplemental Fig. S3*D*, available at www.jneurosci.org as supplemental material) and GFP-PSD-95 ($n = 15$ particles, 3 experiments) (Fig. 3*L*; supplemental Fig. S3*D*, available at www.jneurosci.org as supplemental material) particles, together with the fluorescent dynein subunit mRFP-DIC (Lardong et al., 2009).

Synaptic morphology changes upon functional dynein inhibition in mice resemble the spine phenotype upon transgenic NLG1 overexpression

To perform loss-of-function *in vivo* and to interfere with dynein-mediated retrograde transport of endogenous NLG at adult stages (1 year), we analyzed mice that transgenically overexpress dynamitin (LaMonte et al., 2002) (supplemental Fig. S4*A*, available at www.jneurosci.org as supplemental material) under the postnatally active Thy1.2 promoter, thereby inhibiting dynein function (supplemental Fig. S4*B*, available at www.jneurosci.org as supplemental material) (LaMonte et al., 2002). This promoter is active in the brain, especially in the cerebellum of these mice (see Fig. 5*C–F*). In agreement with NLG1 and PSD-95 packets comigrating with dynein (Fig. 3*K–N*), inhibition of retrograde-directed dynein transport caused a significant accumulation of both NLG1/3 (wt: 0.85 ± 0.15; tg: 3.22 ± 0.22, $n = 3$ experiments/animal, $p < 0.001$) (Fig. 4*A*) and PSD-95 (wt: 1.07 ± 0.28; tg: 1.99 ± 0.06, $n = 3$ experiments/animal, $p < 0.05$) (Fig. 4*B*) in postsynaptic density preparations derived from transgenic (tg), as compared to wild-type (wt), mice. In contrast, the control analysis of whole-cell extracts from both genotypes revealed equal levels of NLG1/3 and PSD-95 (NLG1/3: wt 0.70 ± 0.23, tg 0.70 ± 0.39; PSD-95: wt 3.08 ± 0.78, tg 3.12 ± 0.74. $n = 3$ experiments/animal) (Fig. 4*C*), confirming that the above results (Fig. 4*A*,*B*) were due to protein redistributions and not to changes in gene expression. Further controls confirmed the specificity of the identified changes, since the subcellular localization of other transmembrane (N-cadherin, GluR1) or submembrane (nNOS) PSD-proteins remained unaltered (Fig. 4*D*).

To check for synapse morphology changes in dynamitin-overexpressing mice, electron microscopy (EM) analysis was applied on ultrathin cerebellar tissue sections derived from wt and

←

studied in the brain of this mouse line, nor is any early lethality known. DAPI staining (blue) labels nuclei. Note that the mosaic expression pattern of the Thy 1.2-driven transgene displays a very prominent dynamitin-flag staining in cerebellum, as compared to hippocampus. DG, Dentate gyrus; CA3, CA3 region; wm, white matter; gcl, granule cell layer; ml, molecular layer. Scale bars, 200 μm. Boxed regions are magnified to the right. White arrows depict cerebellar Purkinje cells. ***E***, Quantification of dynamitin-flag expression in hippocampus and cerebellum of transgenic mice using the software MetaMorph. The relative signal intensities of hippocampal dynamitin-flag are significantly lower than in the cerebellum (hippocampus: 0.80 ± 0.64 relative intensity; cerebellum: 6.26 ± 2.85 relative intensity, Student's *t* test: 2.61×10^{-5}, 3 transgenic animals, 3 sections/first animal, 3 sections/s animal, 4 sections/third animal). ***F***, Immunohistochemical detection of dynamitin-flag (red) and calbindin (green) in the cerebellum of tg mice. Wt mice do not express dynamitin-flag. In tg mice, dynamitin-flag expression is seen in Purkinje cells, as verified by colocalization of the calbindin and dynamitin-flag signals (yellow).

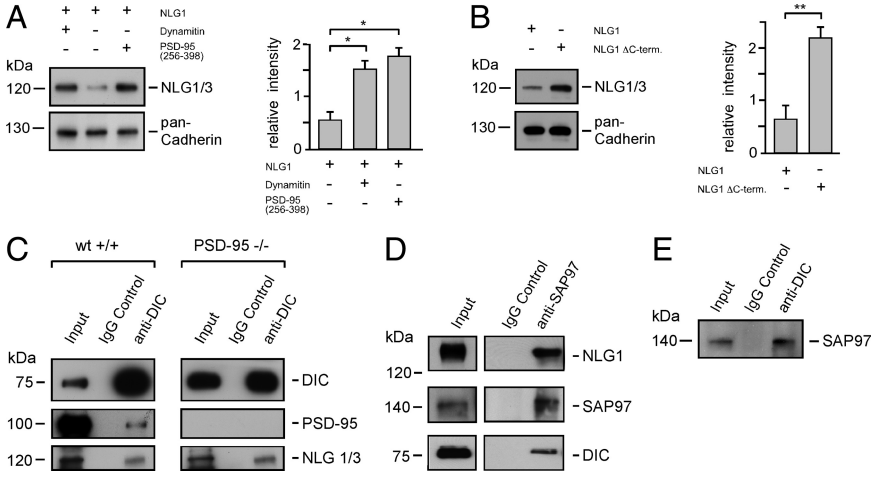

Figure 6. Dynein inhibition (through dynamitin overexpression), a competing PSD-95 peptide, and an NLG1 C-terminal mutant each specifically alter NLG1 surface expression levels in heterologous cells. ***A***, ***B***, Quantitative biotinylation analysis of NLG1 surface localization (HEK293 cells). Interestingly, these cells do not endogenously express PSD-95, but they do endogenously express several other PDZ domain-containing proteins (compare with supplemental Fig. S4*D*, available at www.jneurosci.org as supplemental material). Blockade of dynein-mediated transport through dynamitin overexpression, competitive interference with the NLG1 C-terminal PDZ binding motif through GFP-PSD-95 (256–398) expression, and deletion of the C-terminal 6 aa in NLG1 (NLGΔC-term.) each significantly increase NLG1 at the cell surface. Pan-cadherin, Loading control. Values reflect relative Western blot signal intensities of surface membrane NLG1/3 protein levels, analyzed using the ImageJ software. ***C***, Coimmunoprecipitation with DIC-specific antibodies on P3 vesicle-enriched brain lysate derived from wild-type (wt +/+) or PSD-95 mutant (PSD-95 −/−) mice (Migaud et al., 1998). DIC associates with NLG1/3 in the absence of PSD-95, known to bind NLG1 with its third PDZ domain. ***D***, ***E***, Other MAGUK-family members also associate with components of the dynein motor complex and compensate the loss of PSD-95. ***D***, SAP97-specific antibodies coprecipitate NLG1 and DIC using wild-type P3 vesicle-enriched brain lysates. ***E***, DIC-specific antibodies coprecipitate SAP97 using wild-type P3 vesicle-enriched brain lysates. Error bars represent the SEM. $*p < 0.05$; $**p < 0.01$.

tg genotypes. Postsynaptic sites from wt tissue revealed an average PSD length of 347 ± 10 nm ($n = 130$). In contrast, the PSD lengths of synapses derived from tg tissue turned out to be significantly increased with 398 ± 8 nm ($n = 159$, $p < 0.001$) on average (Fig. 5*A*). Spine head area measurements confirmed this view, displaying significantly larger spine heads in tissue derived from tg animals (187,543 + 5995 nm^2; $n = 119$, $p < 0.001$) than in wt tissue (136,346 + 9526 nm^2; $n = 102$) (Fig. 5*B*). Consistently, control analysis in the hippocampus, a region characterized by low expression of the flag-tagged transgene (Fig. 5*C*,*E*), did not exhibit these specific changes (supplemental Fig. S4*C*, available at www.jneurosci.org as supplemental material). Upon the inhibition of dynein motors, which transport multiple cargoes, it is expected that other proteins can also be redistributed. However, it is notable that the observed cerebellar morphology changes upon local NLG1/3 enrichment (Fig. 4*A*, *B*) resemble the spine morphology phenotype of transgenic mice that exclusively overexpress NLG1 (Dahlhaus et al., 2010) (compare with Fig. 5).

Specific interference with neuroligin dynamics through peptide competition and deletion mutagenesis

To meet concerns that dynein inhibition affects multiple cargoes in parallel, we next aimed to apply peptide competition and mutagenesis for specific loss-of-function experiments that interfere with the formation of the individual protein complex analyzed. First, we applied a biotinylation assay upon heterologous myc-NLG1 expression to directly measure surface NLG1 levels (HEK293 cells), either under control conditions or in the presence of (1) dynamitin, (2) a competitive peptide PSD-95 (256–398) harboring the PDZ3 domain that interferes with NLG1-PSD-95 binding, or (3) an NLGΔC-terminal mutant [unable to bind to PSD-95 (Irie et al., 1997)], respectively. Notably, all conditions significantly increased cell surface NLG1 levels, with relative signal intensities being approximately threefold to fourfold higher than control levels (Fig. 6*A*,*B*) (*A*: myc-NLG1: 0.56 ± 0.25; myc-NLG1+ dynamitin: 1.52 ± 0.28; myc-NLG1+ PSD-95 (256–398): 1.73 ± 0.28; $n = 4$ experiments, $p < 0.05$; *B*: myc-NLG1: 0.68 ± 0.29; myc-NLG1ΔC-term.: 2.24 ± 0.23; $n = 4$ experiments, $p < 0.01$). This indicates that either blocking of retrograde transport or removing NLG's connection to the retrograde motor retains NLG1 at the plasma membrane. Interestingly, this assay worked in HEK293 cells, although the cell line does not endogenously express PSD-95, but expresses several other PDZ domain-containing proteins (supplemental Fig. S4*D*, available at www.jneurosci.org as supplemental material). This prompted us to repeat the previously performed co-IP experiment with DIC-specific antibodies (compare with Fig. 3*E*) on vesicle-enriched brain lysates (P3) from PSD-95 mutant mice, lacking synaptic full-length PSD-95 (Migaud et al., 1998). Notably, in the absence of a PSD-95 protein containing its third PDZ domain (Migaud et al., 1998) (PSD-95 −/−), important for neuroligin binding, NLG1/3 was still subject to coprecipitation with DIC (Fig. 6*C*). This indicates that PSD-95, albeit a component of the complex, is not essential for neuroligin–dynein interactions. Alternatively, since PSD-95 is a member of the MAGUK family (Davies et al., 2001), containing other homologous family members that also bind NLG1 (Meyer et al., 2004), compensatory effects are likely to account for this observation. Analysis of other MAGUK family members (PSD-93, SAP97, and SAP102) revealed that these proteins are clearly present at PSD-95-deficient PSDs (not shown) with SAP102 further known to be upregulated upon the loss of PSD-95 (Cuthbert et al., 2007). Moreover, co-IP with SAP-97-specific antibodies revealed coprecipitation of DIC and NLG1/3 (Fig. 6*D*) and DIC-specific antibodies also coprecipitated SAP97 (Fig. 6*E*), indicating that other MAGUKs indeed associate with the dynein-NLG1 complex. This suggests that PSD-95 is an optional component of the complex, likely to be exchangeable through other PDZ-domain-containing MAGUK family members.

Due to dynein's role in endosomal sorting/transport (Traer et al., 2007) and with the aim to transfer the competitive peptide and the neuroligin mutant into a neuronal context, we then applied an internalization assay upon myc-NLG1 expression in cultured hippocampal neurons. Internalized NLGs (red) appeared in a cytoplasmic, vesicular fraction, while remaining surface proteins stained blue (Fig. 7*A*). Within 2 h, 16.45 ± 1.74% ($n = 3$ experiments) of NLG1 was internalized (Fig. 7*B*). From this fraction, 64.51 ± 4.08% of the particles colocalized with the early endosome antigen EEA1 (Fig. 7*C–E*). In contrast, high sucrose, known to block endocytosis (Kittler et al., 2000), inhibited cytoplasmic NLG1 accumulation (1.00 ± 0.19%, $n = 3$ experiments, $p < 0.001$) (Fig. 7*A*,*B*). First the assay was combined with overexpression of either dynamitin-EGFP or the competitive GFP-PSD-95 fragment [GFP-PSD-95 (256–398)] (Fig. 7*A*,*B*). Control whole-cell patch-clamp recordings revealed that dynamitin-EGFP-overexpressing neurons display resting (E_r) and action (AP)

potentials similar to untransfected neurons (GFP expression: E_r −57.1 ± 1.2 mV, AP 76.8 ± 3.0 mV, $n = 11$ neurons; dynamitin-EGFP expression: E_r −54.2 ± 2.9 mV, AP 71.1 ± 5.4 mV, $n = 9$ neurons), indicating that the applied experimental conditions were not neurotoxic. While dynamitin overexpression functionally inhibits dynein transport (Burkhardt et al., 1997), GFP-PSD-95 (256–398) aimed to specifically compete with NLG/PSD-95 binding. Indeed, both conditions significantly reduced NLG1 internalization rates to 4.53 ± 0.62% and 4.41 ± 0.60%, respectively ($n = 3$ experiments, $p < 0.001$) (Fig. 7*B*). Also, deletion of the very C-terminal PDZ binding motif (HSTTRV) in myc-NLG1 (NLGΔC terminus), required for MAGUK binding (Irie et al., 1997; Meyer et al., 2004), resulted in highly significant reductions in NLG1 internalization (1.60 ± 0.48%, $n = 6$ experiments, $p < 0.001$) (Fig. 7*B*). As a further control, the analysis of AMPA receptor GluR2 subunit internalization in EGFP and dynamitin-EGFP-expressing neurons revealed no difference in the amount of internalized GluR2 between the two conditions (EGFP: 93.63 ± 1.80 arbitrary intensity units; $n = 20$ cells, 4 experiments and dynamitin-EGFP: 95.39 ± 1.99 arbitrary intensity units; $n = 23$ cells, 5 experiments), thereby reflecting the results obtained above (Fig. 4*D*). Together these data show that, in addition to dynein inhibition, competitive interference with NLG-PSD-95 binding or deletion of the NLG1 C terminus interferes with NLG1 endocytosis, with endocytic processes in turn known to require dynein retrograde transport (Driskell et al., 2007; Traer et al., 2007).

Discussion

In summary, our data show for the first time that NLGs undergo protein turnover in an LTP/LTD- (Fig. 1), microtubule- (Fig. 2*E*,*F*), and motor protein-dependent (Figs. 3–7) manner. Recent data have revealed that the normal expression of LTP in the amygdala requires NLG1 (Kim et al., 2008) and that NLG1 cooperates with NMDA receptors to regulate input-specific synaptic plasticity in the amygdala (Jung et al., 2010). Consistent with long-term plasticity modulating higher-order network functions, the loss of NLG1 in mice resulted in impaired spatial memory and increased repetitive behavior (Blundell et al., 2010). Postsynaptic NLG1 further participates in retrograde signaling (Futai et al., 2007) underlying the regulation of presynaptic maturation (Wittenmayer et

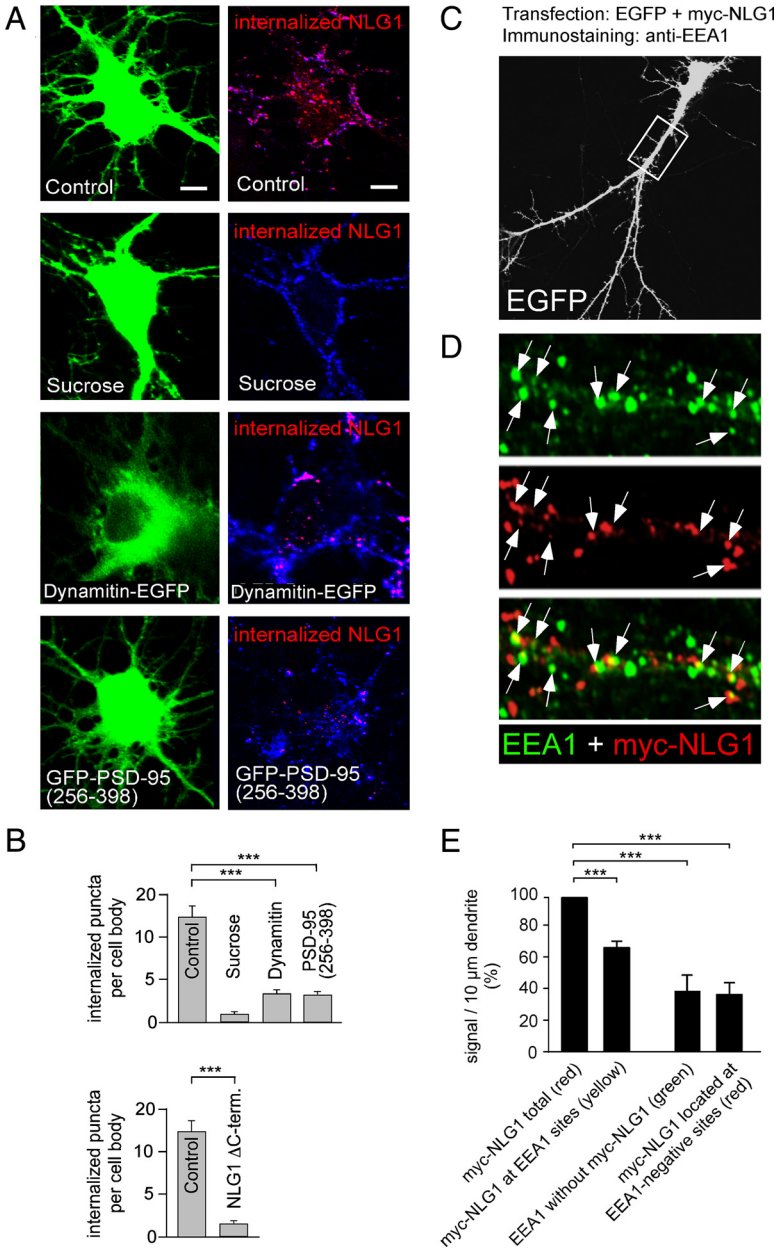

Figure 7. Dynein inhibition (through dynamitin overexpression), a competing PSD-95 peptide, and an NLG1 C-terminal mutant each specifically interfere with NLG1 internalization in neurons. ***A***, ***B***, Neuronal internalization assay using myc-NLG1. Expression of EGFP, dynamitin-EGFP, or the competitive peptide GFP-PSD-95 (256–398) (green) is shown. Surface membrane myc-NLG1 is shown in blue and internalized myc-NLG1 in red. High sucrose prevents myc-NLG1 internalization. Blockade of dynein-mediated transport through dynamitin-EGFP overexpression, competitive interference with the NLG1 C-terminal PDZ binding motif through GFP-PSD-95 (256–398) expression, and deletion of the C-terminal 6 aa in NLG1 (NLGΔC-term.) each significantly reduce myc-NLG1 internalization in neurons ($p < 0.001$). Values reflect numbers of fluorescent signals of internalized myc-NLG1, analyzed using the MetaMorph software. Scale bar, 8 µm. Error bars represent the SEM. ***$p < 0.001$. ***C***, ***D***, Internalized myc-NLG1 colocalizes with EEA1, a marker of the endocytic pathway. We applied a neuronal internalization assay using myc-NLG1 (control experiment to ***A***, ***B***) with subsequent immunodetection of the early endosomal marker protein EEA1. As a transfection control, cells were cotransfected with EGFP. For a better visualization of merged puncta, EEA1 (as originally detected in the blue channel) is shown in a false color (green). Myc-NLG1 is shown in red. EGFP is shown in white. ***C***, EGFP channel. ***D***, EEA1 and myc-NLG1 channels as a magnification of the boxed area in ***C***. Note that 16.45 ± 1.74% of NLG1-myc is internalized in the time period analyzed (compare with ***B***). Yellow colocalized puncta indicate that internalized myc-NLG1 enters the endocytic pathway (arrows). Green puncta represent early endosomes that are negative for myc-NLG1. Red puncta represent internalized myc-NLG1-positive structures other than early endosomes (e.g., late endosomes, recycling endosomes, lysosomes). ***E***, Quantification of ***D***. Of internalized myc-NLG1 signals, 64.51 ± 4.08% colocalize with EEA1 (yellow). Of EEA1-positive puncta, 38.0% ± 10.58% do not colocalize with internalized myc-NLG1 (green). Of internalized myc-NLG1 puncta, 35.49 ± 7.64% do not colocalize with EEA1 (red). Values reflect numbers of fluorescent signals of internalized myc-NLG1, analyzed using the MetaMorph software. Error bars represent the SEM. ***$p < 0.001$.

al., 2009) and synaptic vesicle accumulation (Stan et al., 2010). In addition to NLGs regulating LTP and behavior, we found here that LTP in turn regulates the postsynaptic surface membrane accumulation of NLG1. NLG surface levels increase upon cLTP and decrease upon cLTD induction. The latter effect is prevented upon microtubule depolymerization. Together with our findings that cLTD induction increases the mobility of NLG1 particles and that NLG1 associates with the dynein motor complex, our data suggest a signaling cascade that mediates cross talk between synaptic transmission and intracellular transport. Activation of CaMKIIα through NMDA receptor (NMDAR)-mediated Ca^{2+} influx has been shown to phosphorylate the tail domain of the microtubule motor KIF17, thereby releasing its cargo, the NMDAR (Guillaud et al., 2008). Activity-dependent posttranslational modifications of motor proteins are therefore candidate mechanisms to also regulate synaptic transport of cell adhesion molecules such as the NLG–dynein complex, as reported in the present study.

NLGs associate with a PSD-95/dynein transport complex (Fig. 3) and leave the neuronal plasma membrane (Figs. 1, 7) or postsynaptic sites (Fig. 2*A*), respectively. Our data do not exclude that additional proteins participate in this protein complex formation and show that PSD-95 is exchangeable through the MAGUK-family protein SAP97. However, selective loss-of-function data through inhibition of the retrograde, but not the anterograde, transport direction (*in vivo* and *in vitro*), as well as specific peptide competition and mutagenesis, to separate NLG1 from dynein, cause postsynaptic or surface membrane enrichment of NLG1 (Figs. 4, 6*A*,*B*, 7). Notably, NLG1 particle mobility in spines occurred at dendritic protrusions that were not subject to retraction. Furthermore, synaptic NLG enrichment upon dynein inhibition was seen in adult mice (1 year), indicating that NLG turnover is not restricted to early stages of neuronal development. It will therefore be interesting to investigate the precise signaling mechanisms that alter intracellular NLG transport in the regulation of synaptic plasticity in adult neuronal networks.

Although the submembrane compartment right underneath the lipid bilayer is rich in actin filaments, internalization of transmembrane proteins has also been shown to involve microtubule-based transport (Gekle et al., 1997), and microtubules were identified to enter spines in an activity-dependent manner (Hu et al., 2008; Jaworski et al., 2009). A recent study demonstrated that endosomal maturation uses endosome movement along microtubules, a process that requires dynein-mediated functions (Driskell et al., 2007). Studies on transferrin receptor (TfnR) internalization revealed that sorting/transport to late endosome compartments represents a two-step process, with dynein participating in the second step that represents internalization downstream of the sorting endosome (Traer et al., 2007). In accordance with the view that dynein also internalizes synaptic proteins, possibly along microtubules that enter spines upon activity changes (Hu et al., 2008; Jaworski et al., 2009), proteomic screens of synaptosome preparations identified dynein subunits at synapses (Husi et al., 2000; Schrimpf et al., 2005). Although the initial steps of plasma membrane internalization seem to be independent of microtubule-based processes and likely use actin-based motors (Driskell et al., 2007; Traer et al., 2007), loss-of-function experiments that interfere with retrograde microtubule transport clearly interfere with NLG1 internalization (Fig. 4*A*), thereby causing morphological consequences at spines that resemble the spine morphology phenotype upon transgenic NLG1 overexpression in mice (Fig. 5) (Dahlhaus et al., 2010). NLG1 internalization therefore likely involves retrograde microtubule transport, although retrograde transport does not generally represent internalization, as it further participates in a number of long-distance cargo rearrangements (Caviston and Holzbaur, 2006) (Fig. 3*K*,*L*). It is furthermore notable that the single overexpression of PSD-95 has led to an increased size of spine heads (compare with Fig. 5*B*), accompanied by multiple innervation of spines (Nikonenko et al., 2008). This process is mediated through nitric oxide (NO) signaling; however, whether NO signaling contributes to the regulation of transport requires further investigation.

Together, the data presented in this study show that neuroligins are not static transsynaptic components, but are dynamically exchanged at postsynaptic sites. They further support the concept that NLG turnover, driven via active cytoskeleton transport mechanisms, represents a potential process to modulate synaptic signaling and changes in synaptic strength.

References

Barrow SL, Constable JR, Clark E, El-Sabeawy F, McAllister AK, Washbourne P (2009) Neuroligin1: a cell adhesion molecule that recruits PSD-95 and NMDA receptors by distinct mechanisms during synaptogenesis. Neural Dev 4:17.

Blundell J, Blaiss CA, Etherton MR, Espinosa F, Tabuchi K, Walz C, Bolliger MF, Südhof TC, Powell CM (2010) Neuroligin-1 deletion results in impaired spatial memory and increased repetitive behavior. J Neurosci 30:2115–2129.

Burkhardt JK, Echeverri CJ, Nilsson T, Vallee RB (1997) Overexpression of the dynamitin (p50) subunit of the dynactin complex disrupts dynein-dependent maintenance of membrane organelle distribution. J Cell Biol 139:469–484.

Caviston JP, Holzbaur EL (2006) Microtubule motors at the intersection of trafficking and transport. Trends Cell Biol 16:530–537.

Chih B, Engelman H, Scheiffele P (2005) Control of excitatory and inhibitory synapse formation by neuroligins. Science 307:1324–1328.

Cuthbert PC, Stanford LE, Coba MP, Ainge JA, Fink AE, Opazo P, Delgado JY, Komiyama NH, O'Dell TJ, Grant SG (2007) Synapse-associated protein 102/dlgh3 couples the NMDA receptor to specific plasticity pathways and learning strategies. J Neurosci 27:2673–2682.

Dahlhaus R, Hines RM, Eadie BD, Kannangara TS, Hines DJ, Brown CE, Christie BR, El-Husseini A (2010) Overexpression of the cell adhesion protein neuroligin-1 induces learning deficits and impairs synaptic plasticity by altering the ratio of excitation to inhibition in the hippocampus. Hippocampus 20:305–322.

Davies C, Tingley D, Kachar B, Wenthold RJ, Petralia RS (2001) Distribution of members of the PSD-95 family of MAGUK proteins at the synaptic region of inner and outer hair cells of the guinea pig cochlea. Synapse 40:258–268.

Dean C, Scholl FG, Choih J, DeMaria S, Berger J, Isacoff E, Scheiffele P (2003) Neurexin mediates the assembly of presynaptic terminals. Nat Neurosci 6:708–716.

Driskell OJ, Mironov A, Allan VJ, Woodman PG (2007) Dynein is required for receptor sorting and the morphogenesis of early endosomes. Nat Cell Biol 9:113–120.

Ehlers MD (2000) Reinsertion or degradation of AMPA receptors determined by activity-dependent endocytic sorting. Neuron 28:511–525.

Fu Z, Washbourne P, Ortinski P, Vicini S (2003) Functional excitatory synapses in HEK293 cells expressing neuroligin and glutamate receptors. J Neurophysiol 90:3950–3957.

Fuhrmann JC, Kins S, Rostaing P, El Far O, Kirsch J, Sheng M, Triller A, Betz H, Kneussel M (2002) Gephyrin interacts with dynein light chains 1 and 2, components of motor protein complexes. J Neurosci 22:5393–5402.

Fujita A, Kurachi Y (2000) SAP family proteins. Biochem Biophys Res Commun 269:1–6.

Futai K, Kim MJ, Hashikawa T, Scheiffele P, Sheng M, Hayashi Y (2007) Retrograde modulation of presynaptic release probability through signaling mediated by PSD-95-neuroligin. Nat Neurosci 10:186–195.

Gekle M, Mildenberger S, Freudinger R, Schwerdt G, Silbernagl S (1997) Albumin endocytosis in OK cells: dependence on actin and microtubules and regulation by protein kinases. Am J Physiol 272:F668–677.

Goddard CA, Butts DA, Shatz CJ (2007) Regulation of CNS synapses by neuronal MHC class I. Proc Natl Acad Sci U S A 104:6828–6833.

Graf ER, Zhang X, Jin SX, Linhoff MW, Craig AM (2004) Neurexins induce differentiation of GABA and glutamate postsynaptic specializations via neuroligins. Cell 119:1013–1026.

Gray NW, Weimer RM, Bureau I, Svoboda K (2006) Rapid redistribution of synaptic PSD-95 in the neocortex in vivo. PLoS Biol 4:e370.

Guillaud L, Wong R, Hirokawa N (2008) Disruption of KIF17-Mint1 interaction by CaMKII-dependent phosphorylation: a molecular model of kinesin-cargo release. Nat Cell Biol 10:19–29.

Hamill OP, Marty A, Neher E, Sakmann B, Sigworth FJ (1981) Improved patch-clamp techniques for high-resolution current recording from cells and cell-free membrane patches. Pflugers Arch 391:85–100.

Heerssen HM, Pazyra MF, Segal RA (2004) Dynein motors transport activated Trks to promote survival of target-dependent neurons. Nat Neurosci 7:596–604.

Hirokawa N, Takemura R (2005) Molecular motors and mechanisms of directional transport in neurons. Nat Rev Neurosci 6:201–214.

Hu X, Viesselmann C, Nam S, Merriam E, Dent EW (2008) Activity-dependent dynamic microtubule invasion of dendritic spines. J Neurosci 28:13094–13105.

Huber KM, Roder JC, Bear MF (2001) Chemical induction of mGluR5- and protein synthesis–dependent long-term depression in hippocampal area CA1. J Neurophysiol 86:321–325.

Husi H, Ward MA, Choudhary JS, Blackstock WP, Grant SG (2000) Proteomic analysis of NMDA receptor-adhesion protein signaling complexes. Nat Neurosci 3:661–669.

Ichtchenko K, Hata Y, Nguyen T, Ullrich B, Missler M, Moomaw C, Südhof TC (1995) Neuroligin 1: a splice site-specific ligand for beta-neurexins. Cell 81:435–443.

Irie M, Hata Y, Takeuchi M, Ichtchenko K, Toyoda A, Hirao K, Takai Y, Rosahl TW, Südhof TC (1997) Binding of neuroligins to PSD-95. Science 277:1511–1515.

Jaworski J, Kapitein LC, Gouveia SM, Dortland BR, Wulf PS, Grigoriev I, Camera P, Spangler SA, Di Stefano P, Demmers J, Krugers H, Defilippi P, Akhmanova A, Hoogenraad CC (2009) Dynamic microtubules regulate dendritic spine morphology and synaptic plasticity. Neuron 61:85–100.

Jung SY, Kim J, Kwon OB, Jung JH, An K, Jeong AY, Lee CJ, Choi YB, Bailey CH, Kandel ER, Kim JH (2010) Input-specific synaptic plasticity in the amygdala is regulated by neuroligin-1 via postsynaptic NMDA receptors. Proc Natl Acad Sci U S A 107:4710–4715.

Kim J, Jung SY, Lee YK, Park S, Choi JS, Lee CJ, Kim HS, Choi YB, Scheiffele P, Bailey CH, Kandel ER, Kim JH (2008) Neuroligin-1 is required for normal expression of LTP and associative fear memory in the amygdala of adult animals. Proc Natl Acad Sci U S A 105:9087–9092.

Kim MJ, Futai K, Jo J, Hayashi Y, Cho K, Sheng M (2007) Synaptic accumulation of PSD-95 and synaptic function regulated by phosphorylation of serine-295 of PSD-95. Neuron 56:488–502.

Kittler JT, Delmas P, Jovanovic JN, Brown DA, Smart TG, Moss SJ (2000) Constitutive endocytosis of GABAA receptors by an association with the adaptin AP2 complex modulates inhibitory synaptic currents in hippocampal neurons. J Neurosci 20:7972–7977.

LaMonte BH, Wallace KE, Holloway BA, Shelly SS, Ascaño J, Tokito M, Van Winkle T, Howland DS, Holzbaur EL (2002) Disruption of dynein/dynactin inhibits axonal transport in motor neurons causing late-onset progressive degeneration. Neuron 34:715–727.

Lardong K, Maas C, Kneussel M (2009) Neuronal depolarization modifies motor protein mobility. Neuroscience 160:1–5.

Loebrich S, Bähring R, Katsuno T, Tsukita S, Kneussel M (2006) Activated radixin is essential for GABAA receptor alpha5 subunit anchoring at the actin cytoskeleton. EMBO J 25:987–999.

Maas C, Tagnaouti N, Loebrich S, Behrend B, Lappe-Siefke C, Kneussel M (2006) Neuronal cotransport of glycine receptor and the scaffold protein gephyrin. J Cell Biol 172:441–451.

Meyer G, Varoqueaux F, Neeb A, Oschlies M, Brose N (2004) The complexity of PDZ domain-mediated interactions at glutamatergic synapses: a case study on neuroligin. Neuropharmacology 47:724–733.

Migaud M, Charlesworth P, Dempster M, Webster LC, Watabe AM, Makhinson M, He Y, Ramsay MF, Morris RG, Morrison JH, O'Dell TJ, Grant SG (1998) Enhanced long-term potentiation and impaired learning in mice with mutant postsynaptic density-95 protein. Nature 396:433–439.

Mok H, Shin H, Kim S, Lee JR, Yoon J, Kim E (2002) Association of the kinesin superfamily motor protein KIF1Bα with postsynaptic density-95 (PSD-95), synapse-associated protein-97, and synaptic scaffolding molecule PSD-95/discs large/zona occludens-1 proteins. J Neurosci 22:5253–5258.

Nikonenko I, Boda B, Steen S, Knott G, Welker E, Muller D (2008) PSD-95 promotes synaptogenesis and multiinnervated spine formation through nitric oxide signaling. J Cell Biol 183:1115–1127.

Oh MC, Derkach VA, Guire ES, Soderling TR (2006) Extrasynaptic membrane trafficking regulated by GluR1 serine 845 phosphorylation primes AMPA receptors for long-term potentiation. J Biol Chem 281:752–758.

Otmakhov N, Khibnik L, Otmakhova N, Carpenter S, Riahi S, Asrican B, Lisman J (2004) Forskolin-induced LTP in the CA1 hippocampal region is NMDA receptor dependent. J Neurophysiol 91:1955–1962.

Palazzo AF, Joseph HL, Chen YJ, Dujardin DL, Alberts AS, Pfister KK, Vallee RB, Gundersen GG (2001) Cdc42, dynein, and dynactin regulate MTOC reorientation independent of Rho-regulated microtubule stabilization. Curr Biol 11:1536–1541.

Palmer MJ, Irving AJ, Seabrook GR, Jane DE, Collingridge GL (1997) The group I mGlu receptor agonist DHPG induces a novel form of LTD in the CA1 region of the hippocampus. Neuropharmacology 36:1517–1532.

Rogers SW, Hughes TE, Hollmann M, Gasic GP, Deneris ES, Heinemann S (1991) The characterization and localization of the glutamate receptor subunit GluR1 in the rat brain. J Neurosci 11:2713–2724.

Scheiffele P, Fan J, Choih J, Fetter R, Serafini T (2000) Neuroligin expressed in nonneuronal cells triggers presynaptic development in contacting axons. Cell 101:657–669.

Schrimpf SP, Meskenaite V, Brunner E, Rutishauser D, Walther P, Eng J, Aebersold R, Sonderegger P (2005) Proteomic analysis of synaptosomes using isotope-coded affinity tags and mass spectrometry. Proteomics 5:2531–2541.

Setou M, Nakagawa T, Seog DH, Hirokawa N (2000) Kinesin superfamily motor protein KIF17 and mLin-10 in NMDA receptor-containing vesicle transport. Science 288:1796–1802.

Setou M, Seog DH, Tanaka Y, Kanai Y, Takei Y, Kawagishi M, Hirokawa N (2002) Glutamate-receptor-interacting protein GRIP1 directly steers kinesin to dendrites. Nature 417:83–87.

Snyder EM, Philpot BD, Huber KM, Dong X, Fallon JR, Bear MF (2001) Internalization of ionotropic glutamate receptors in response to mGluR activation. Nat Neurosci 4:1079–1085.

Song JY, Ichtchenko K, Südhof TC, Brose N (1999) Neuroligin 1 is a postsynaptic cell-adhesion molecule of excitatory synapses. Proc Natl Acad Sci U S A 96:1100–1105.

Stan A, Pielarski KN, Brigadski T, Wittenmayer N, Fedorchenko O, Gohla A, Lessmann V, Dresbach T, Gottmann K (2010) Essential cooperation of N-cadherin and neuroligin-1 in the transsynaptic control of vesicle accumulation. Proc Natl Acad Sci U S A 107:11116–11121.

Südhof TC (2008) Neuroligins and neurexins link synaptic function to cognitive disease. Nature 455:903–911.

Taniguchi H, Gollan L, Scholl FG, Mahadomrongkul V, Dobler E, Limthong N, Peck M, Aoki C, Scheiffele P (2007) Silencing of neuroligin function by postsynaptic neurexins. J Neurosci 27:2815–2824.

Traer CJ, Rutherford AC, Palmer KJ, Wassmer T, Oakley J, Attar N, Carlton JG, Kremerskothen J, Stephens DJ, Cullen PJ (2007) SNX4 coordinates endosomal sorting of TfnR with dynein-mediated transport into the endocytic recycling compartment. Nat Cell Biol 9:1370–1380.

Vallee RB, Williams JC, Varma D, Barnhart LE (2004) Dynein: an ancient motor protein involved in multiple modes of transport. J Neurobiol 58:189–200.

Varoqueaux F, Aramuni G, Rawson RL, Mohrmann R, Missler M, Gottmann K, Zhang W, Südhof TC, Brose N (2006) Neuroligins determine synapse maturation and function. Neuron 51:741–754.

Wittenmayer N, Körber C, Liu H, Kremer T, Varoqueaux F, Chapman ER, Brose N, Kuner T, Dresbach T (2009) Postsynaptic Neuroligin1 regulates presynaptic maturation. Proc Natl Acad Sci U S A 106:13564–13569.